Published OnlineFirst December 2, 2015; DOI: 10.1158/0008-5472.CAN-15-1610

Therapeutics, Targets, and Chemical Biology

Cancer Research

SLC46A3 Is Required to Transport Catabolites of Noncleavable Antibody Maytansine Conjugates from the Lysosome to the Cytoplasm

Kevin J. Hamblett[1], Allison P. Jacob[1], Jesse L. Gurgel[1], Mark E. Tometsko[1], Brooke M. Rock[2], Sonal K. Patel[2], Robert R. Milburn[3], Sophia Siu[4], Seamus P. Ragan[5], Dan A. Rock[2], Christopher J. Borths[3], Jason W. O'Neill[4], Wesley S. Chang[6], Margaret F. Weidner[1], Matthew M. Bio[3], Kim C. Quon[1], and William C. Fanslow[1]

Abstract

Antibody–drug conjugates (ADC) target cytotoxic drugs to antigen-positive cells for treating cancer. After internalization, ADCs with noncleavable linkers are catabolized to amino acid-linker-warheads within the lysosome, which then enter the cytoplasm by an unknown mechanism. We hypothesized that a lysosomal transporter was responsible for delivering noncleavable ADC catabolites into the cytoplasm. To identify candidate transporters, we performed a phenotypic shRNA screen with an anti-CD70 maytansine-based ADC. This screen revealed the lysosomal membrane protein SLC46A3, the genetic attenuation of which inhibited the potency of multiple noncleavable antibody–maytansine ADCs, including ado-trastuzumab emtansine. In contrast, the potencies of noncleavable ADCs carrying the structurally distinct monomethyl auristatin F were unaffected by SLC46A3 attenuation. Structure–activity experiments suggested that maytansine is a substrate for SLC46A3. Notably, SLC46A3 silencing led to relative increases in catabolite concentrations in the lysosome. Taken together, our results establish SLC46A3 as a direct transporter of maytansine-based catabolites from the lysosome to the cytoplasm, prompting further investigation of SLC46A3 as a predictive response marker in breast cancer specimens. *Cancer Res; 75(24); 5329–40. ©2015 AACR.*

Introduction

Two antibody–drug conjugates (ADC), brentuximab vedotin (1) and ado-trastuzumab emtansine (2), are currently approved for the treatment of cancer. Several ADCs are currently under investigation in clinical trials, many of which employ the same antitubulin agents in brentuximab vedotin and ado-trastuzumab emtansine, auristatins, and maytansinoids, respectively (3). The majority of ADCs in the clinic, including brentuximab vedotin, employ a cleavable linker, which, following internalization and activation within the cell, releases a warhead from the linker. Cleavable linker warheads, such as the maytansinoids DM1 and DM4, and the auristatin monomethyl auristatin E (MMAE), are potent molecules in the single digit nanomolar to picomolar range. Once released, DM1, DM4, and MMAE are capable of bystander activity, killing target-negative cells (4, 5). Two warhead families are well established to generate active ADCs with noncleavable linkers, maytansinoids including DM1 and DM4 (6, 7) and monomethyl auristatin F (8). ADCs with noncleavable linkers kill target cells following a stepwise process of (i) antibody binding to cell surface target, (ii) ADC internalization into the endolysosomal pathway, (iii) catabolism of ADC in the lysosome to liberate amino acid-linker-warhead (9), (iv) catabolite exit from lysosome to cytoplasm, and (v) catabolite interaction with intracellular target. Unlike warheads released from cleavable linker ADCs, catabolites of noncleavable linker ADCs do not penetrate cell membranes and consequently do not generate bystander activity (4). While the generation of amino acid-linker-warhead from noncleavable linker ADCs and their subsequent ability to mediate cell death once in the cytoplasm are well established, the mechanism of noncleavable linker catabolite exit from the lysosome into the cytoplasm is unknown.

Gene silencing (10) is a powerful tool frequently used to define genes important for cell division (11), survival (12), and sensitization of cells to chemotherapy agents (13, 14). In addition, phenotypic screening has been used to identify genes involved in the mechanism of action of molecules (15). To define genes involved in catabolite transport from the lysosome to the cytoplasm, a noncleavable maytansine-based ADC, anti-CD70 Ab-MCC-DM1, was evaluated in positive selection phenotypic shRNA screens that identified solute carrier family 46 member

[1]Amgen Inc., Therapeutic Innovation Unit, Seattle, Washington. [2]Amgen Inc., Pharmacokinetics and Drug Metabolism, Seattle, Washington. [3]Amgen Inc., Small Molecule Purification and Process Development, Thousand Oaks, California. [4]Amgen Inc., Therapeutic Discovery, Seattle, Washington. [5]Amgen Inc., Genome Analysis Unit, Seattle, Washington. [6]Amgen Inc., Clinical Immunology, South San Francisco, California.

Note: Supplementary data for this article are available at Cancer Research Online (http://cancerres.aacrjournals.org/).

K.J. Hamblett and A.P. Jacob contributed equally to this article.

Current address for K.J. Hamblett: Zymeworks Biopharmaceuticals, 18 West Mercer St., Seattle, WA 98119.

Corresponding Author: Kevin J. Hamblett, Amgen, 1201 Amgen Court West, Seattle, WA 98119. Phone: 206-237-1031; E-mail: kjhamblett@comcast.net

doi: 10.1158/0008-5472.CAN-15-1610

Published OnlineFirst December 2, 2015; DOI: 10.1158/0008-5472.CAN-15-1610

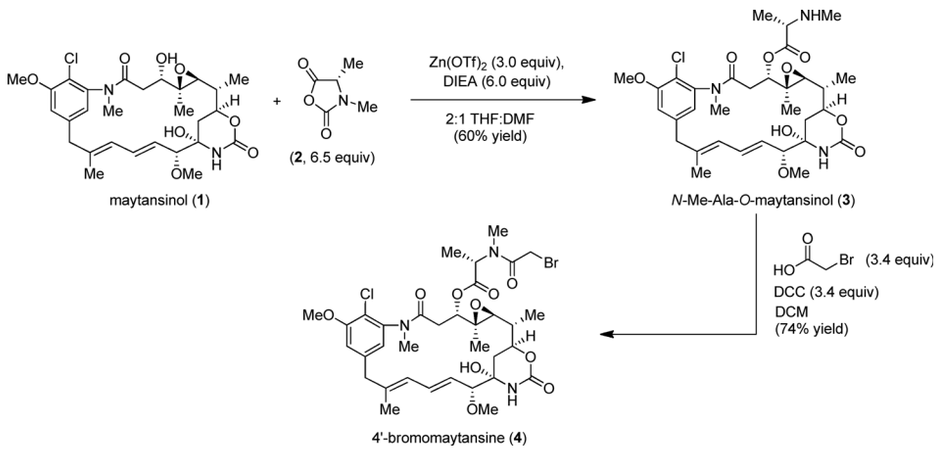

Scheme 1.
Synthesis of 4′-bromomaytansine.

A3 (SLC46A3). Validation experiments using different linker-warhead systems and cell surface targets demonstrated that SLC46A3 regulates the lysosomal concentration of the Ab-MCC-DM1 catabolite Lysine-MCC-DM1. These results support a role for SLC46A3 in the transport of the noncleavable linker ADC catabolite Lysine-MCC-DM1 from the lysosome into the cytoplasm.

Materials and Methods

Cell lines

786-0 cells were originally obtained from ATCC and passaged in RPMI + 10% FBS. U251vIII cells were obtain from Dr. Darell Bigner (Duke University, Durham, NC) and passaged in DMEM + 10% FBS. SK-BR-3 cells were obtained from ATCC and were passaged in McCoys + 10% FBS. Cell lines were not authenticated.

Reagents

Synthesis of 4′bromomaytansine. *Scheme 1.* Maytansinol (**1**, 0.10 g, 1.0 equiv) and benzene (1.0 mL) were charged to a round bottom flask. The solution was concentrated to an oil and backfilled with $N_{2(g)}$ to dry the flask and contents (repeated × 3). *N*,*N*-dimethylformamide (0.5 mL), tetrahydrofuran (1.0 mL), *N*,*N*-diisopropylethylamine (0.19 mL, 3.0 equiv), and a magnetic stirbar were charged to the flask at ambient temperature to generate a slightly yellow homogeneous solution. (*S*)-3,4-dimethyloxazolidine-2,5-dione (**2**, 0.114 g, 5.0 equiv) was charged to the solution, followed by zinc trifluoromethanesulfonate (0.193 g, 3.0 equiv) to generate a heterogeneous mixture, which was sealed and aged overnight at ambient temperature. The following day, an additional 1.5 equiv of (*S*)-3,4-dimethyloxazolidine-2,5-dione (0.034 g) was charged to the mixture, and the slurry was aged overnight at ambient temperature. The reaction was quenched by charging 2.0 mL 10% ethylenediaminetetraacetic acid aq. solution (1.1 equiv relative to $zinc^{+2}$) and 2.0 mL 5 mol/L sodium chloride aq. solution. The aqueous layer was extracted with ethyl acetate (4.0 mL × 2), and the combined ethyl acetate extract was washed with 2.0 mL 5 mol/L sodium chloride solution. The ethyl acetate solution was dried over anhydrous sodium sulfate, concentrated, and purified by silica chromatography (100% dichloromethane to 10% methanol:dichloromethane) to provide 98 mg of *N*-Me-Ala-*O*-maytansinol (**3**) as a yellow oil in 60% potency adjusted yield.

N-Me-Ala-*O*-maytansinol (**3**, 65 mg, 1.0 equiv), dichloromethane (1.7 mL), and a magnetic stirbar were charged to a round bottom flask. *N*,*N*-Dicyclohexylcarbodiimide (70 mg, 3.4 equiv) and 2-bromoacetic acid (47 mg, 3.4 equiv) were sequentially charged to form a white slurry, and the flask was sealed and aged overnight at ambient temperature. The slurry was purified by silica chromatography (2% methanol:dichloromethane) to provide 63 mg of 4′-bromomaytansine (**4**) as a white powder in 74% potency adjusted yield.

Synthesis of N-Me-Ala-O-maytansinol-DSG-NHS. *Scheme 2.* *N*-Me-Ala-*O*-maytansinol (**3**, 5.6 mg, 8.61 μmol), bis(2,5-dioxopyrrolidin-1-yl) glutarate (**5**, 14.05 mg, 5.0 equiv), and *N*,*N*-dimethylpyridin-4-amine (1.052 mg, 1.0 equiv) were charged to a vial

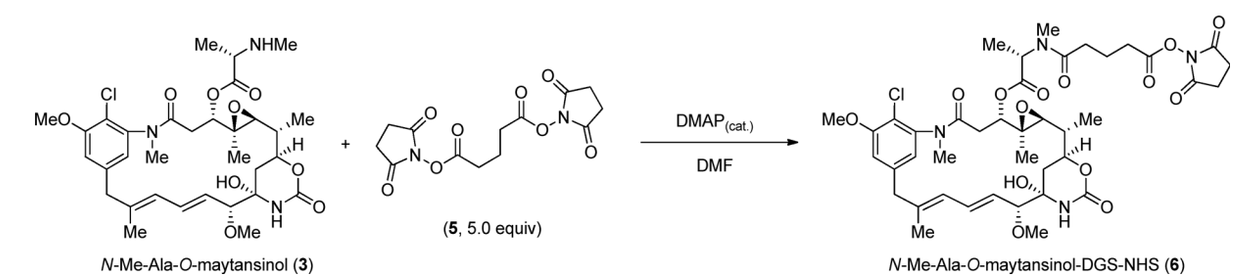

Scheme 2.
Synthesis of *N*-Me-Ala-*O*-maytansinol-DSG-NHS.

Published OnlineFirst December 2, 2015; DOI: 10.1158/0008-5472.CAN-15-1610

Scheme 3.
Synthesis of DM1-SMCC.

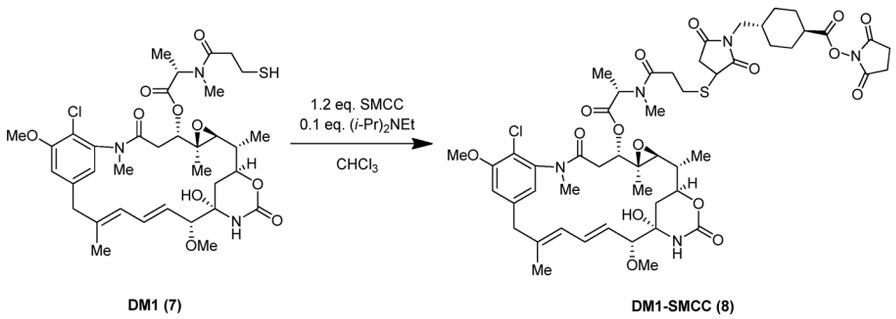

containing a magnetic stirbar. DMF (100 μL) was charged to the vial to generate a homogeneous solution, and the vial was sealed and aged overnight at ambient temperature. Upon reaction completion, 1.0 mL ethyl acetate and 2.0 mL 5% sodium chloride aq. solution was charged. The phases were separated, and the aqueous phase was extracted with 1.0 mL ethyl acetate. The combined organic phases were washed with brine, dried with anhydrous sodium sulfate, concentrated, and purified by silica chromatography (3% methanol:dichloromethane to 5% methanol:dichloromethane) to provide *N*-Me-*O*-maytansinol-DGS-NHS (**6**) as an oil.

Synthesis of DM1-SMCC. *Scheme 3.* DM1 (**7**, 1081 mg, 1.27 mmol), SMCC (512 mg, 1.53 mmol), diisopropylethylamine (22.2 μL, 0.127 mmol), and dry chloroform (21.6 mL) were charged to a 100 mL round bottom flask equipped with a magnetic stir bar. The mixture was stirred at room temperature under an atmosphere of nitrogen overnight. The mixture was concentrated to a residue at 40°C and reduced pressure on a rotovap to yield a solid residue. The residue was purified by preparative HPLC (Luna Silica, 21.2 × 150 mm, 5 μm column; 20 mL/minute isocratic elution; 20% acetonitrile/MTBE) to yield 994 mg of DM1-SMCC (**8**) as a white solid (73% yield, potency adjusted).

Generation of ADC

Anti-EGFRvIII Ab-MCC-DM1 was conjugated as previously described (16). Anti-EGFRvIII Ab-mcMMAF and anti-CD70 Ab-mcMMAF were generated as previously (8) described using mcMMAF (The Chemistry Research Solutions).

Anti-CD70 antibody was conjugated to DM1-SMCC (**8**) to generate anti-CD70 Ab-MCC-DM1. Briefly, anti-CD70 antibody in 50 mmol/L potassium phosphate, 2 mmol/L EDTA, pH 7.5 was mixed with a 12-fold molar excess of DM1-SMCC in dimethylacetamide (DMAC) at room temperature for 90 minutes, followed by 4°C overnight incubation. Final anti-CD70 Ab-MCC-DM1 had a drug–antibody ratio (DAR) of 4.8.

Anti-CD70 Ab-DSG-maytansine was generated by conjugating anti-CD70 antibody to *N*-Me-Ala-*O*-maytansinol-DSG-NHS (**6**). Briefly, anti-CD70 antibody in 50 mmol/L NaCl, 2 mmol/L EDTA, pH 8.5 was mixed with a 5-fold molar excess of *N*-Me-Ala-*O*-maytansinol-DSG-NHS at room temperature for 90 minutes, followed by 4°C overnight incubation. Final anti-CD70 Ab-DSG-maytansine had a DAR of 4.4.

Anti-CD70 Ab-Cys-maytansine was generated by conjugating a site-specific cysteine mutant of the anti-CD70 antibody with 4′-bromomaytansine (**4**). Briefly, anti-CD70 Ab-Cys was reduced with tris(2-carboxyethyl)phosphine hydrochloride (TCEP) for 2 hours at room temperature. Excess TCEP was removed by amicon spin columns. (L)-Dehydroascorbic Acid (DHAA) was added to reoxidize native disulfide bonds for 2 hours at room temperature. A 10-fold molar excess of 4′-bromomaytansine was added to the reduced antibody for 2 hours to generate anti-CD70 Ab-Cys-Maytansine with a DAR of 1.8.

For generation of trastuzumab-MCC-DM1 conjugate DM1 was purchased from Carbosynth to generate DM1-SMCC as described above. Trastuzumab in conjugation buffer (50 nmol/L boric acid, 50 mmol/L NaCl, 2 mmol/L EDTA, pH 8.5 was mixed at room temperature with DM1-SMCC (**8**) in DMAC for 70 minutes. The ADC was buffer exchanged to 10 mmol/L sodium acetate, 9% sucrose, 0.01% PS20, pH 5.0 using a 10 mL 7 kDa Zeba Spin desalting column according to the manufacturer's instructions. Trastuzumab-MCC-DM1 had a DAR of 3.9.

shRNA library synthesis, screening, and statistcal analysis

shRNA libraries 1 and 2 were designed to target 1,276 and 1,325 genes, respectively. Libraries were synthesized by Cellecta with an average of 19 and 18 shRNAs per gene for libraries 1 and 2, respectively. Each shRNA was synthesized with a unique barcode. Both libraries included shRNAs to 30 genes with no cell growth phenotype after knockdown, and 17 genes previously demonstrated as essential for cell growth for internal controls (data not shown). For screens, 786-0 cells were transduced with lentiviral packaged shRNAs at 3,000 cells/shRNA at an MOI of 0.3 such that the majority of infectants contained single integrations. Transduced cells were selected in puromycin. One thousand cells/shRNA were exposed to ADC for 96 hours and remaining cells were expanded for an additional 96 hours in the absence of ADC. Cells were harvested and barcodes were PCR-amplified and sequenced using an Illumina sequencer (Cellecta Inc) as previously described (17). The number of reads of each shRNA barcode was normalized to reads per 40 million total reads (the typical read depth in each experiment) to correct for variations in read depth in each experiment. shRNAs with fewer than 50 reads per 40 million in the control arm were excluded from analysis. The effect of each shRNA on ADC function was quantified using the value: log[(reads/40 million ADC-treated experiment)/(reads/40 million untreated experiment)]. The values for duplicate shRNAs were averaged to generate a single value for each shRNA. The approximately 18 to 19 independent shRNAs/gene were used to estimate a *P* value for each gene as previously described (18), which was then used to calculate a *q*-value corrected for multiple hypothesis testing using the method of Hochberg and Benjamini (19).

Published OnlineFirst December 2, 2015; DOI: 10.1158/0008-5472.CAN-15-1610

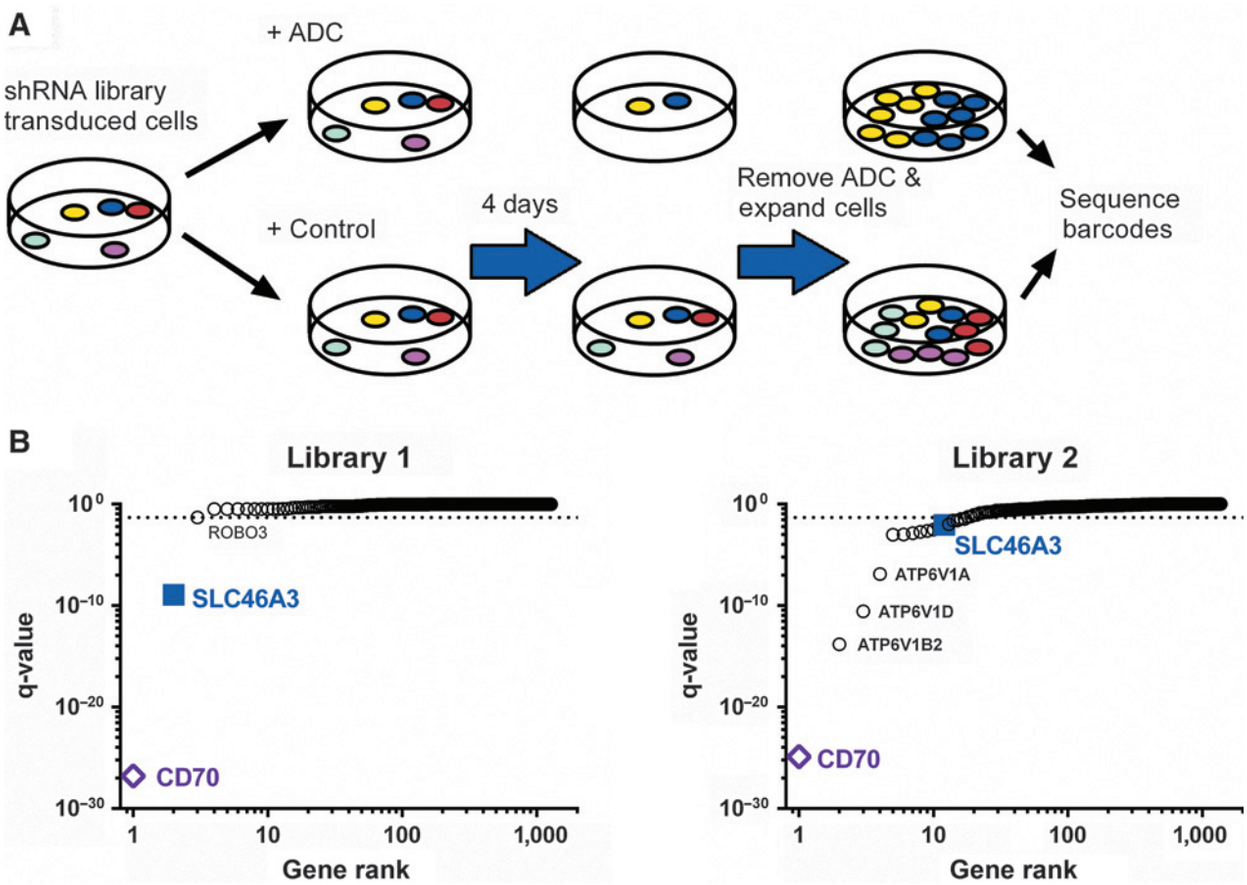

Figure 1.
shRNA screen overview and results. A, 786-0 cells were transduced with the shRNA library and expanded. shRNA library–transduced cells were treated with anti-CD70 Ab-MCC-DM1 or media (control) for four days. Cells were washed and replated for another four days to expand remaining cells in the absence of ADC. Cells were collected for bar code sequencing. B, library 1 and library 2 *q*-value plotted as a function of gene rank; line indicates *q* value of 0.05.

Cell viability experiments

Cells were transfected with 3 to 4 independent siRNA sequences per gene, each independent siRNA was assayed in either duplicate or triplicate. Forty-eight hours after transfection, cells were exposed to ADC. Cell growth was either monitored continuously by Incucyte (Essen BioScience) or after 72 hours ADC exposure using Cell Titer Glo (Promega). Luminescence was measured using an Envision plate reader (Perkin Elmer).

Lysine-MCC-DM1 concentration

Lysine-MCC-DM1 concentration in cell lysate and lysosomes was assessed in 786-0 cells in a 6-well plate as previously described (9). For siRNA experiments, 24 hours after plating cells, 5 nmol/L SLC46A3-specific or nontargeting siRNA in OptiMEM and RNAi Max was added to cells (Life Technologies). Twenty-four hours later, the medium was removed and replaced with 10% RPMI. After 24 hours, 786-0 cells were treated with 3 or 10 nmol/L anti-CD70 antibody-MCC-DM1, based on DM1 concentration. Plates were placed in an Incucyte or in a standard incubator, which at various times media was removed and cells were frozen for total lysate generation or used to isolate lysosomes followed by liquid chromatography/tandem mass spectrometry (LC/MS-MS) measurement of Lysine-MCC-DM1 as previously described (9).

Statistical analysis

Comparison of siRNA effect on cell viability following ADC exposure was determined using one-way ANOVA with Tukey multiple comparisons correction. Comparison of lysosomal Lysine-MCC-DM1 concentrations normalized to total lysate Lysine-MCC-DM1 concentration (Fig. 4B) was determined using a *t* test. ANOVA and *t* tests were performed in GraphPad Prism version 6.05.

Results

shRNA screens identified CD70 and SLC46A3 as critical mediators of anti-CD70 Ab-MCC-DM1–dependent cytotoxicity

Cell surface target expression and lysosomal function have been shown to be critical for the potency of noncleavable linker of ADCs (6, 8). Anti-CD70 Ab-MCC-DM1 is a potent noncleavable linker ADC targeting the cell surface protein CD70, which is expressed on the renal cell carcinoma line 786-0. Screens employing two distinct custom shRNA libraries were performed to identify genes involved in noncleavable linker maytansine ADC (anti-CD70 Ab-MCC-DM1) catabolite transport from the lysosome to cytoplasm. Library 1 contained genes annotated as membrane proteins, predominantly cell surface proteins, while

Published OnlineFirst December 2, 2015; DOI: 10.1158/0008-5472.CAN-15-1610

library 2 was designed to include genes annotated to have transporter function or lysosomal localization (20–22), approximately 35 amino acid transporter genes, and genes that regulate lysosomal function consisting of 14 lysosmal ATPase subunits. The shRNA libraries were screened in 786-0 cells using cell survival as a readout (Fig. 1A). A hit was defined as (i) significantly different q-value of anti-CD70 Ab-MCC-DM1 relative to cells under normal growth conditions and (ii) a membrane protein with either unknown function or known transporter function, excluding lysosomal ATPase subunits, which transport H+ into lysosomes. As expected, given the target specific nature of the anti-CD70 Ab-MCC-DM1, CD70 was the most significant gene in both screens with q-values of 1.59×10^{-27} and 1.30×10^{-25} in libraries 1 and 2, respectively (Fig. 1B). Genes involved in endosomal/lysosomal trafficking (Rab7A), lysosomal biogenesis (mTor), and lysosomal function (multiple ATPase subunits, V1B2, V1D, V1A, and V0C) were identified in the screens, but not defined as hits (Supplementary Tables S1 and S2). A number of proteins identified in the screens were not classified as hits due to nonmembrane localization, including ribosomal protein components (RPL3, RPS6, and RPS3A). SLC46A3, a lysosomal membrane protein (21) with unknown function, was the only hit identified with q-values of 1.18×10^{-9} and 9.01×10^{-3} in libraries 1 and 2, respectively (Fig. 1B). SLC46A3 is a member of the major facilitator superfamily, with highest homology to its subfamily of solute carrier family members SLC46A1 and SLC46A2 (33% and 27%, respectively). SLC46A1 is expressed in intestine, brain, and kidney, and transports folate in a proton-dependent manner (23). SLC46A2 is expressed in thymic epithelia and the epididymal duct, but its substrates have not been identified (24, 25). RNA sequence analysis of normal tissue indicated SLC46A3 is expressed at low levels in 786-0 cells as well as most tissues (26, 27). The predicted structure for SLC46A3 suggests it contains 12 transmembrane spanning domains (Supplementary Fig. S1), similar to SLC46A1 (28) and SLC46A2 (24). Identification of a solute carrier family member localized in the lysosomal membrane warranted

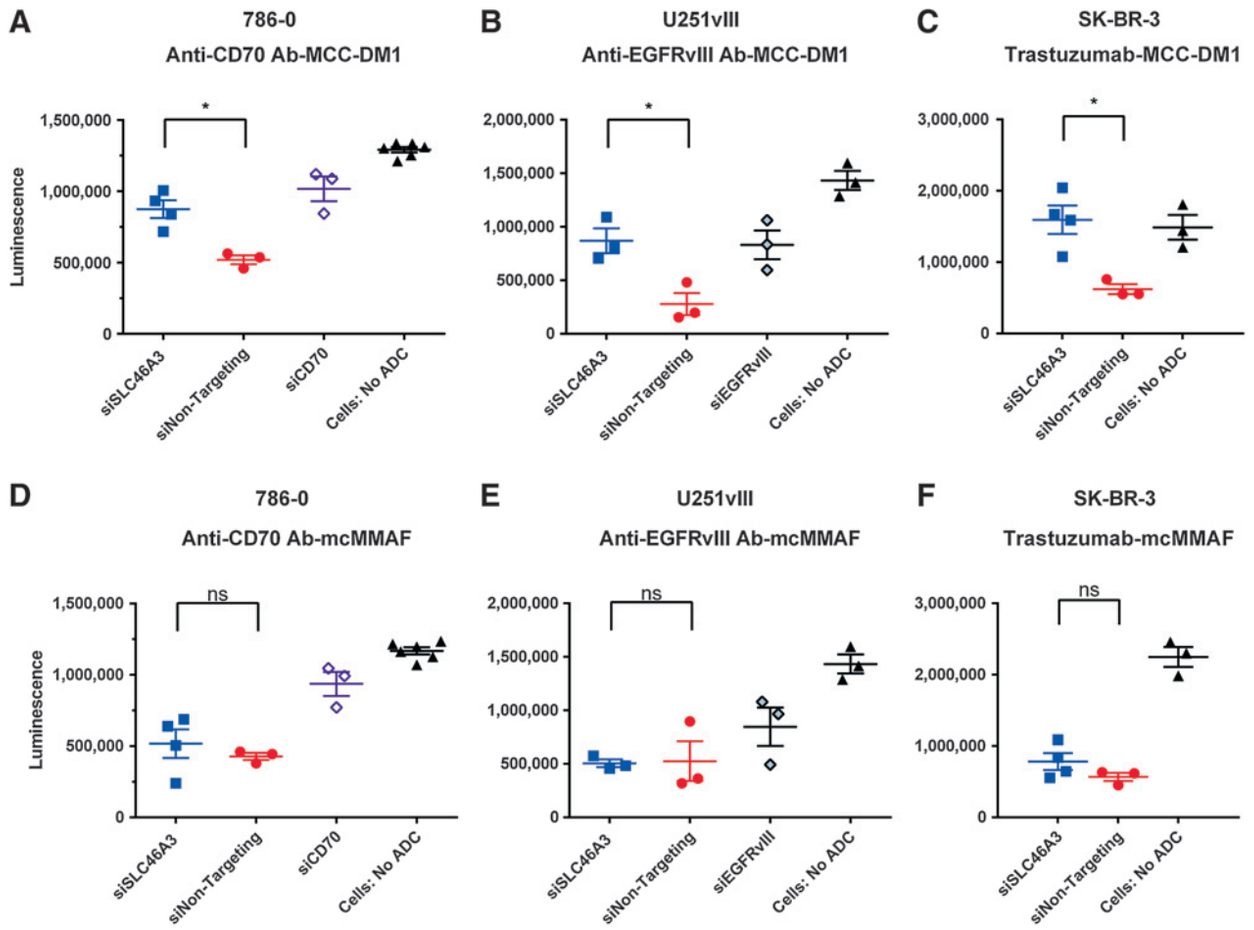

Figure 2.
SLC46A3 siRNA affect on Ab-MCC-DM1 and Ab-mcMMAF conjugates. CD70-expressing 786-0 cells (A and D), EGFRvIII-expressing U251vIII cells (B and E), and HER2-expressing SK-BR-3 cells (C and F) were transfected with multiple independent siRNA sequences against SLC46A3, CD70, EGFRvIII, or nontargeting. Twenty-four hours after transfection, cells were exposed to anti-CD70 Ab-MCC-DM1 (A), anti-EGFRvIII Ab-MCC-DM1 (B), trastuzumab-MCC-DM1 (C), anti-CD70 Ab-mcMMAF (D), anti-EGFRvIII Ab-mcMMAF (E), or trastuzumab-mcMMAF (F) for three days, followed by measurement of cell viability by CellTiter-Glo. Each siSLC46A3, siNon-targeting, siEGFRvIII, and siCD70 point represents an independent siRNA sequence average of either duplicates or triplicates. Bars represent the mean cell viability in the presence of independent siRNA sequences treated with ADC or cells ± SEM. Statistical test for significance utilized a one-way ANOVA with multiple comparisons correction, *, $P < 0.05$; ns, not significant. Representative experiments are shown.

Published OnlineFirst December 2, 2015; DOI: 10.1158/0008-5472.CAN-15-1610

additional experimentation of SLC46A3 to validate its role in noncleavable linker ADC catabolite transport.

SLC46A3 is required for maytansine-based noncleavable ADC activity and is independent of cell surface target

To verify SLC46A3's role in noncleavable linker ADC mechanism of action, gene expression was knocked down in 786-0 cells using highly selective siRNAs in the presence of anti-CD70 Ab-MCC-DM1. CD70-specific siRNAs reduced mRNA levels of CD70 (Supplementary Fig. S2), surface expression of CD70 (Supplementary Fig. S3), and, as expected, reduced the potency of anti-CD70 Ab-MCC-DM1 (Fig. 2A). siRNA-mediated reduction of SLC46A3 expression was evaluated using mRNA expression (Supplementary Fig. S2), as commercially available antibodies were not specific or sensitive enough to detect endogenous levels of SLC46A3. Figure 2A demonstrates that siRNA knockdown of SLC46A3 mRNA attenuates the potency of anti-CD70 Ab-MCC-DM1 compared with nontargeting siRNAs. To characterize the breadth of SLC46A3's role in noncleavable linker ADC mechanism of action, two additional ADCs each directed against a

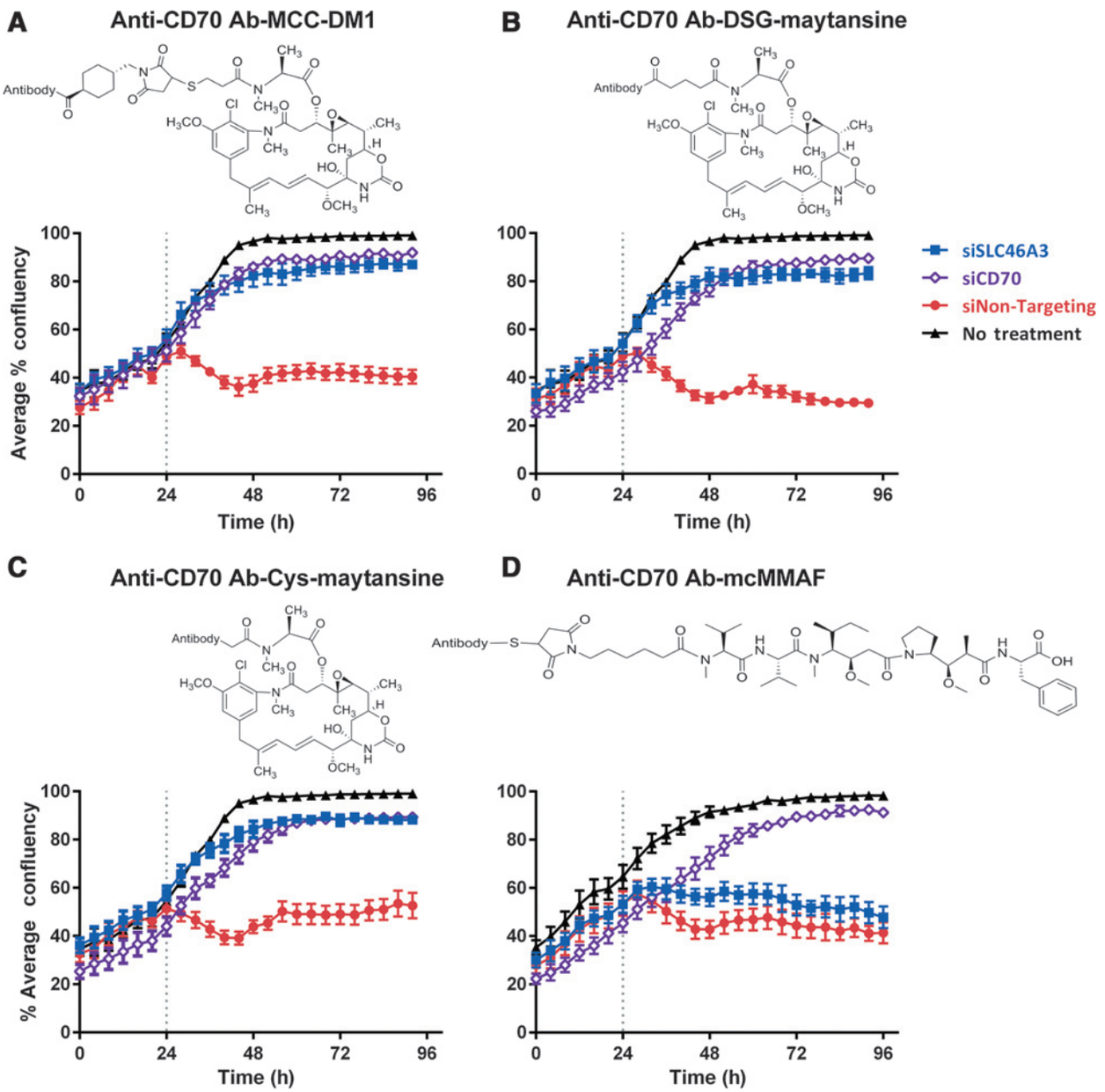

Figure 3.
SLC46A3 siRNA validation and assessment of different ADCs. 786-0 cells in 96-well plates were transfected with independent siRNAs: SLC46A3 ($n = 4$), CD70 ($n = 4$), nontargeting ($n = 4$), or no siRNA ($n = 3$). Twenty-four hours after transfection, cells were incubated with anti-CD70 Ab-MCC-DM1 (A), anti-CD70 Ab-DSG-maytansine (B), anti-CD70 Ab-Cys-maytansine (C), or anti-CD70 Ab-mcMMAF (D). Average cell confluency ± SEM is graphed. The relevant linker-warhead structures are shown in each panel. Representative experiments are shown.

Published OnlineFirst December 2, 2015; DOI: 10.1158/0008-5472.CAN-15-1610

different cell surface target employing the same noncleavable linker technology, anti-EGFRvIII Ab-MCC-DM1 and ado-trastuzumab emtansine (trastuzumab-MCC-DM1) were evaluated on target-expressing tumor cells to determine whether the effect of SLC46A3 on ADC function was cell surface target or cell line specific. EGFRvIII is a deletion mutant of exons 2–7 of EGFR (29). The potency of anti-EGFRvIII Ab-MCC-DM1 against U251vIII cells (Fig. 2B) and trastuzumab-MCC-DM1 against SK-BR-3 cells (Fig. 2C) were attenuated by selective SLC46A3 mRNA knockdown, establishing that the role of SLC46A3 affecting Ab-MCC-DM1 potency is not specific to a cell surface target or cell line.

SLC46A3 is required for maytansine-based noncleavable warhead ADC potency but not auristatin-based noncleavable warhead ADC potency

To address the hypothesis that SLC46A3 is involved in maytansine-based catabolite transport from the lysosome to the cytoplasm ADCs utilizing the noncleavable linker warhead MMAF were generated. Anti-CD70 Ab-mcMMAF potency in 786-0 cells was unaffected by selective SLC46A3 knockdown (Fig. 2D). Similar to anti-CD70 Ab-mcMMAF, neither anti-EGFRvIII Ab-mcMMAF (Fig. 2E) nor trastuzumab-mcMMAF (Fig. 2F) were affected by selective SLC46A3 knockdown in U251vIII or SK-BR-3 cells, respectively, suggesting that a distinct structural element within lysine-MCC-DM1 is recognized by SLC46A3.

To determine whether structural elements of the linker in anti-CD70 Ab-MCC-DM1 are important for recognition by SLC46A3, the linker between maytansine and the anti-CD70 antibody was replaced with a simple glutaric acid spacer. A bis-activated glutaric acid was first reacted with maytansine then the anti-CD70 antibody to generate anti-CD70 Ab-DSG-maytansine, which is catabolized to lysine-DSG-maytansine. Potency of anti-CD70 Ab-DSG-maytansine was similar to anti-CD70 Ab-MCC-DM1 (Supplementary Fig. S4) demonstrating that cyclohexane in MCC is not a critical component for ADC potency. Knockdown of SLC46A3 attenuated the potency of anti-CD70 Ab-DSG-maytansine compared with nontargeting siRNA (Fig. 3B), similar to the attenuation observed with anti-CD70 Ab-MCC-DM1 (Fig. 3A) indicating that the linker component was unlikely recognized by SLC46A3. Cysteines are frequently used to conjugate auristatins and other drugs to antibodies, thus, maytansine was conjugated directly to an engineered site-specific cysteine of the anti-CD70 antibody to determine the effect of SLC46A3 on a different amino acid present in the catabolite. The resulting anti-CD70 Ab-Cys-maytansine is catabolized into Cys-maytansine in the cell, and is potent against 786-0 cells (Supplementary Fig. S4). The potency of anti-CD70 Ab-Cys-maytansine was attenuated upon knockdown of SLC46A3 (Fig. 3C), indicating SLC46A3 function is not specific to the lysine residue attached to the maytansine species. Similar to the endpoint assay (Fig. 2D), anti-CD70 Ab-mcMMAF potency was attenuated by knockdown of CD70 similar to the maytansine-based ADCs. However, in contrast to the maytansine ADCs, the anti-CD70 Ab-mcMMAF potency was not affected by SLC46A3 knockdown (Fig. 3D). These results, specifically the lack of sensitivity to the linker or amino acid component of the catabolites, suggest that SLC46A3 recognizes maytansine or a moiety within the maytansine scaffold.

Lysine-MCC-DM1 concentration in the lysosome transiently peaks twelve hours following treatment of anti-CD70 Ab-MCC-DM1

Methods were recently developed to measure lysine-MCC-DM1 by LC/MS-MS in total cell lysates and the lysosomal fractions of mammalian cells to assess the intracellular fate of noncleavable linker ADCs (9). 786-0 cells treated with anti-CD70 Ab-MCC-DM1 generated low yet measurable levels of the ADC catabolite lysine-MCC-DM1 6 hours after treatment with the ADC. The total cell lysate concentration of lysine-MCC-DM1 increased as a

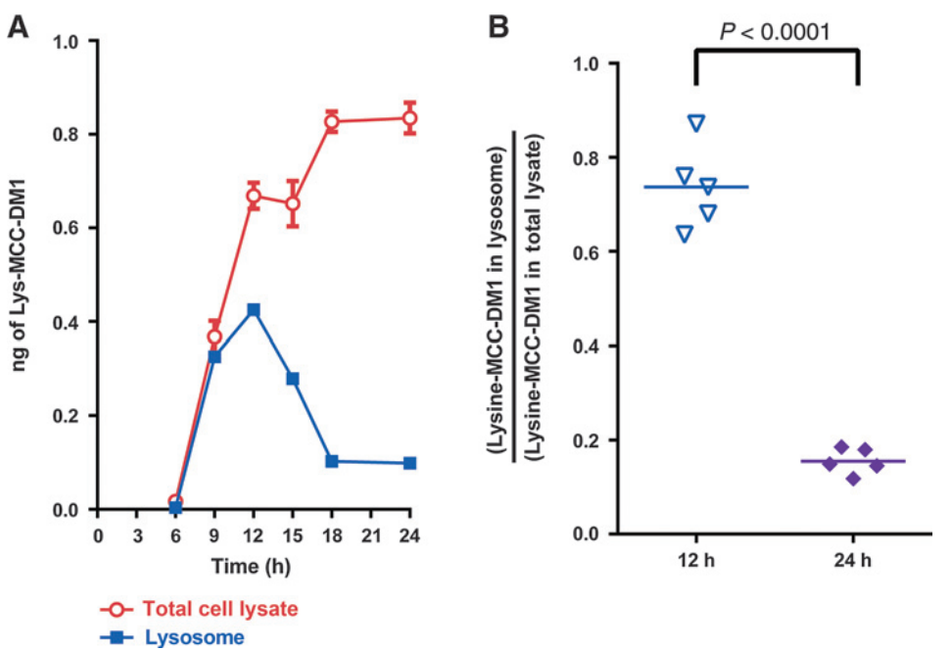

Figure 4.
Lysine-MCC-DM1 kinetics in cell lysate and lysosome. 786-0 cells were treated with anti-CD70 Ab-MCC-DM1; at specific time points, total cell lysate or lysosomes were collected. Cells were frozen after the ADC incubation period, followed by solubilization in ethyl acetate to generate total cell lysate (red open circles; $n = 3 \pm$ SEM). Live cells were harvested and lysosomes extracted using a lysosome extraction kit (blue squares; $n = 1$ per time point). Lysine-MCC-DM1 concentration was measured by LC/MS-MS. A, time course of total lysate and lysosome from a representative experiment. B, lysine-MCC-DM1 concentration in the lysosome normalized to total lysate at 12 and 24 hours; statistical test for significance utilized a *t* test.

Published OnlineFirst December 2, 2015; DOI: 10.1158/0008-5472.CAN-15-1610

function of time in culture with the ADC (Fig. 4A), continuing through 48 hours (Supplementary Fig. S5). Within the lysosome the concentration of lysine-MCC-DM1 had a distinctly different profile than the total cell lysate. Nine hours after ADC treatment the concentration of lysine-MCC-DM1 in the lysosome was similar to the total cell lysate concentration (Fig. 4A). Twelve hours after ADC treatment, the lysosomal concentration of Lysine-MCC-DM1 peaked and was approximately 3.5-fold higher than at 24 hours. Lysine-MCC-DM1 concentration in the lysosome decreased from 12 to 18 hours, after which the levels stabilized. Lysosome levels of Lysine-MCC-DM1 were significantly higher at 12 hours compared with 24 hours ($P < 0.0001$) as shown in Fig. 4B.

SLC46A3 knockdown attenuates the postpeak decrease of lysine-MCC-DM1 concentration in the lysosome following anti-CD70 Ab-MCC-DM1 treatment

To determine the functional role of SLC46A3 knockdown the concentration of the catabolite lysine-MCC-DM1 was measured in the total cell lysate and lysosome in the presence of the selective siRNA knockdown of SLC46A3 mRNA or nontargeting siRNA knockdown following anti-CD70 Ab-MCC-DM1 treatment. Despite the larger cell numbers required for lysine-MCC-DM1 concentration measurements, siSLC46A3-mediated knockdown attenuated the potency of anti-CD70 Ab-MCC-DM1 (Supplementary Fig. S6) to a similar extent to that observed in smaller scale experiments (Fig. 3A). Total cell lysate lysine-MCC-DM1 concentration was comparable between cells exposed to nontargeting and SLC46A3 siRNAs at both the 12-hour and 24-hour timepoints (Fig. 5A and C). Twelve hours after treatment with anti-CD70 Ab-MCC-DM1, the lysosomal concentration of lysine-MCC-DM1 was similar to the total cell lysate concentration in cells exposed to both SLC46A3 and nontargeting siRNAs (Fig. 5B relative to Fig. 5A and Fig. 5D relative to Fig. 5C). After twenty-four hour treatment with anti-CD70 Ab-MCC-DM1, the lysosomal concentration of lysine-MCC-DM1 was markedly higher in cells where selective SLC46A3 mRNA knockdown occurred as compared with cells exposed to nontargeting siRNA, indicating a direct role for SLC46A3 in regulation of the lysosomal concentration of lysine-MCC-DM1 (Fig. 5B and D).

Discussion

Technology improvements during the past decade, including improved warheads (1), linker stability (30, 31), optimization of drug loading (32), and the in the case of ado-trastuzumab emtansine, noncleavable linker technology (30) contributed to the approval of two ADCs for clinical use. With hydrazone, disulfide, and protease-based cleavable linkers the warheads typically used are drugs with robust potency against a wide range of cells, such as doxorubicin (33), MMAE (8), and maytansinoids (34) DM1 and DM4. These warheads are hypothesized to freely diffuse across cell membranes and the lysosomal membrane (5, 35). Noncleavable linker ADCs generate warheads still attached to amino acids, most notably cysteine-mcMMAF or lysine-MCC-DM1, depending on the technology employed, which were hypothesized to not readily diffuse across cell membranes (36). One ADC that employs maytansine-based noncleavable linker technology is ado-trastuzumab emtansine (30). Ado-trastuzumab emtansine (trastuzumab-MCC-DM1) significantly improves overall survival in metastatic breast cancer patients (2), yet, one key aspect of its mechanism of action, how the ADC catabolite lysine-MCC-DM1 exits the lysosome and enters the cytoplasm, remains unknown.

To elucidate genes involved in transport of the noncleavable linker ADC catabolite lysine-MCC-DM1 from the lysosome to the cytoplasm two shRNA libraries containing approximately 2,600 genes were screened employing a cell line exposed to anti-CD70 Ab-MCC-DM1. Functional screening with shRNA can be a powerful tool, however, prior screens using 3 to 7 shRNAs per gene have been confounded by the frequency of false positives (37). Using ricin susceptibility as a model, Bassik and colleagues examined the number of shRNAs required to resolve significant *P* values for both weak and strong hits (38). Consequently, two distinct shRNA libraries were designed consisting of 1,276 and 1,325 genes, in library 1 and library 2 respectively, with approximately 18 to 19 shRNAs per gene. As expected, the ADC cell surface target, CD70, was the most significant gene identified in both screens, while SLC46A3, a gene member in the same family of membrane transporters yet with unknown function, was the only other gene identified in both screens.

Transporters play a role in the cellular influx and efflux of multiple pharmaceutical drugs (39), xenobiotics, amino acids, and other small molecules such as folate. The development of genomic screens has validated, and in some cases discovered, transporters that deliver certain drugs into cells. A genome-wide assessment of 26 pharmaceutical drugs in yeast identified the transporters for 18 compounds that when deleted impacted potency (40). Two studies using genetic screens identified transporters that played a role in the potency of the nucleoside antibiotic tunicamycin (41) and the anticancer agent YM155 (42). The transporters identified in these examples were cell surface transporters affecting the potency of small molecules. SLC46A3 represents the first lysosomal transporter identified that is necessary for the function of a noncleavable linker maytansine-based ADC.

Maytansine-based noncleavable linker ADC potency was significantly impacted by knockdown of SLC46A3. By evaluating the effects of SLC46A3 knockdown on Ab-MCC-DM1 and Ab-mcMMAF on different cell surface targets (Fig. 2) we demonstrate that SLC46A3 represents a broad underlying mechanism of maytansine ADCs with noncleavable linkers, not merely a cell line or cell surface target–specific phenomenon. SLC46A3 likely recognizes the macrolide structure of maytansine as neither linker structure nor a different amino acid impacted the ADC potency attenuation of SLC46A3 knockdown (Fig. 3). MMAF, the only other extensively characterized noncleavable linker warhead, when delivered into cells as an ADC was not significantly impacted by SLC46A3 knockdown. Maytansine's macrolide structure is distinctly different from the pentapeptide MMAF, thus it is reasonable that if SLC46A3 is functioning as a transporter, only one of these distinctly different structures would be a substrate for SLC46A3. Potency of the MMAF ADCs were unaffected by SLC46A3 knockdown, strongly suggesting the existence of a distinct transport mechanism of Cys-mcMMAF from the lysosome into the cytoplasm. To functionally validate SLC46A3 in its native environment, we measured lysine-MCC-DM1 concentration in the lysosome. Measurement of lysine-MCC-DM1 in the lysosome by LC/MS-MS is a technically challenging low-throughput endeavor, typically generating $n = 1$ per condition or timepoint. Despite the low sample size, the inter-assay coefficient of variation (%CV) ranged between 8% and 15%, indicating the precision of the assay measurements. SLC46A3 knockdown did not affect the cumulative rate of internalization, trafficking to

Published OnlineFirst December 2, 2015; DOI: 10.1158/0008-5472.CAN-15-1610

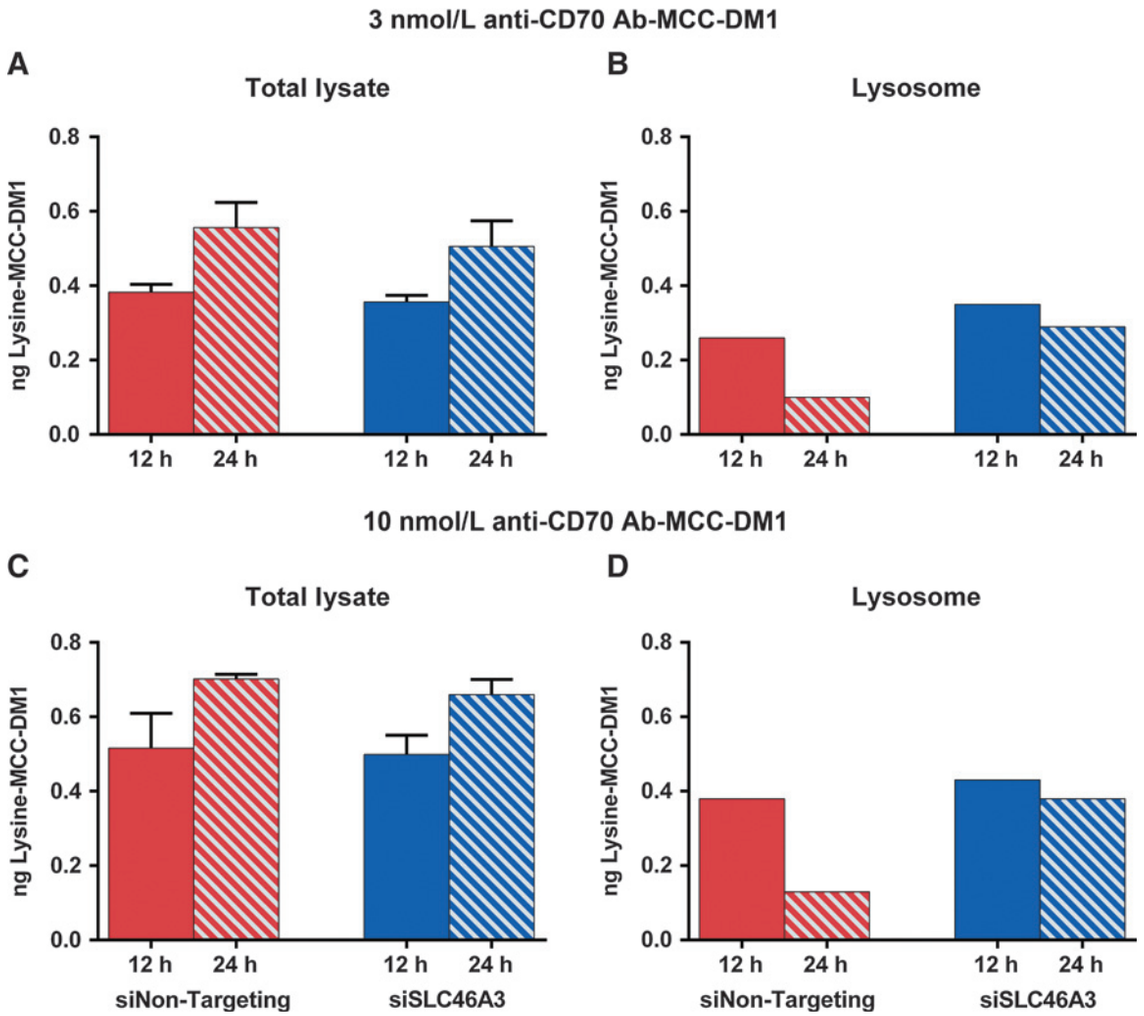

Figure 5.
Functional effect of SLC46A3 on lysine-MCC-DM1 concentration. 786-0 cells were transfected with nontargeting or SLC46A3 siRNAs. Twenty-four hours after transfection, cells were treated with 3 nmol/L (A and B) or 10 nmol/L (C and D) anti-CD70 Ab-MCC-DM1 for 12 or 24 hours. Total cell lysate ($n = 3 \pm$ SEM; A and C) or lysosomes ($n = 1$ per time point; B and D) were collected and lysine-MCC-DM1 concentration measured by LC/MS-MS.

lysosomes, and catabolism of anti-CD70 Ab-MCC-DM1 into lysine-MCC-DM1 as evidenced by the similar total cell lysate concentrations of lysine-MCC-DM1 with either siSLC46A3 or nontargeting siRNA at both 12 and 24 hours (Fig. 5A and C). While lysine-MCC-DM1 accumulated in the lysosome upon SLC46A3 knockdown at 24 hours it did not reach the concentration of the total cell lysate, suggesting either incomplete knockdown of SLC46A3 with siRNA, or perhaps another transporter capable of transporting lysine-MCC-DM1 from the lysosome to cytoplasm, or another mechanism. While the SLC46A3 knockdown led to lysosomal accumulation of lysine-MCC-DM1 has a limited number of biologic replicates the inter-assay precision of the lysosome concentration measurement suggests that the accumulation observed at 24 hours is robust and reproducible. In future studies it would be of interest to assess the lysosomal accumulation of lysine-MCC-DM1 following ADC treatment in the complete absence of SLC46A3 expression. Our experimental results show that SLC46A3 is necessary for transport of lysine-MCC-DM1 from the lysosome to the cytoplasm following ADC catabolism to enable on-target inhibition of tubulin polymerization. This data is summarized in a model for noncleavable linker maytansine ADCs in Fig. 6, where upon lysosomal catabolism SLC46A3 transports catabolites into the cytoplasm.

Of the three SLC46 family members, substrates have only been identified for SLC46A1, also known as the proton coupled folate transporter, which transports folate (23), and to a lesser extent heme (43), from the lumen of the jejunum and duodenum into cells in a pH-dependent fashion as it is expressed on the apical membrane (44). SLC46A1 was not found to be enriched in any of the shRNA screens performed, suggesting that it does not recognize and transport lysine-MCC-DM1, or lacked the relevant cofactor in the screen, thus it is unknown if SLC46A1 and SCL46A3 may share substrates. Other families of transporters, such as Nramp (45) and the SLC15 (46) families, contain genes where one or more members is/are expressed in the gut and another member is expressed in the lysosome. In these cases, the transporters in both the gut and the lysosome transport molecules in a pH-dependent fashion. Furthermore, substrates can be shared

Published OnlineFirst December 2, 2015; DOI: 10.1158/0008-5472.CAN-15-1610

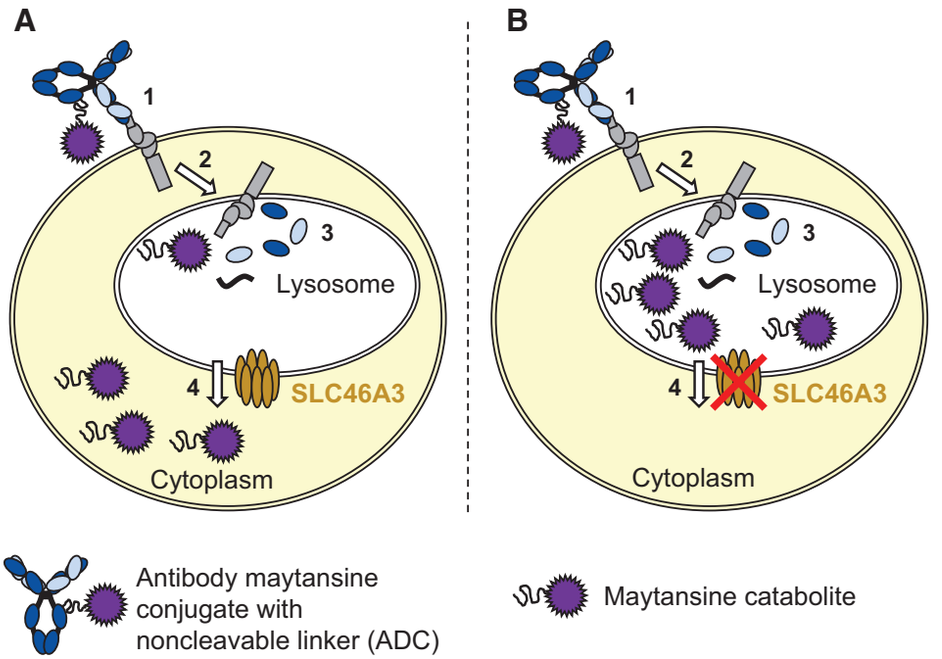

Figure 6.
Proposed model of noncleavable antibody maytansine conjugate. In a cell with wild-type SLC46A3 (A) and a cell with SLC46A3 knocked down (B), the mechanism of noncleavable antibody maytansinoid conjugates are similar for steps 1–3. Antibody conjugate binding to the cancer cell surface target (1); conjugate internalization into the endolysosomal pathway (2); catabolism of conjugate to amino acid-linker-warhead catabolite (3). For the final step (4), catabolite transport from lysosome into cytoplasm occurs in cells with wild-type SLC46A3 (A), but is attenuated when SLC46A3 is knocked down, leading to lysosomal accumulation (B).

among family members despite expression on different membranes. Attempts to direct the lysosomal-localized Nramp1 to the cell surface by swapping the N- and C-terminal domains of Nramp1 with the cell surface–localized Nramp2 were unsuccessful (47). However, Nramp2 was localized to lysosomes when its N terminus was replaced with the N-terminus of Nramp1, suggesting that Nramp1 may contain multiple lysosomal sorting motifs. Multiple modifications to SLC46A3's proposed lysosomal sorting motifs (48) to force expression on the cell surface were unsuccessful as single mutations (data not shown), suggesting that similar to Nramp1 SLC46A3 may contain multiple lysosomal localization sorting motifs. Without a cell surface assay, it is challenging to validate that SLC46A3 alone is sufficient to transport lysine-MCC-DM1 across membranes or to determine any cofactors required for transport such as pH. Evaluation of pH as a cofactor for lysosomal transport following ADC treatment is complicated by the observation that proton pump inhibitors such as bafilomycin prevent the formation of lysine-MCC-DM1 (9), presumably the lysosomal proteases that catabolize antibodies are pH dependent. Nevertheless, the identification of SLC46A3 as a lysosomal membrane protein (21), the specificity of SLC46A3 for maytansine-based ADCs, and observation that SLC46A3 impacts the lysosomal concentration of lysine-MCC-DM1 (Fig. 5B and D) suggests that SLC46A3 is either a lysosomal transporter or directly involved in the transport of lysine-MCC-DM1 from lysosome to cytoplasm.

Cleavable linker ADCs exhibit potency with multiple warheads including auristatins (1), maytansinoids (36) such as DM1 and DM4, doxorubicin (33), calicheamicins (49), and pyrrolobenzodiazepines (50), whereas noncleavable linker ADCs are reported to be successful only with maytansines and the auristatin MMAF. Knockdown of SLC46A3 significantly attenuated the potency of ADCs that employed noncleavable maytansine-based warheads including anti-CD70 Ab-MCC-DM1, anti-EGFRvIII Ab-MCC-DM1, and ado-trastuzumab emtansine, an approved treatment for metastatic breast cancer. Attenuation of ado-trastuzumab emtansine potency upon SLC46A3 knockdown *in vitro*, suggests that similar consequences could occur in patients that may harbor a defect in SLC46A3 levels or function. Little is known about the potential effects of SLC46A3 polymorphisms, yet, interrogation of clinical samples could clarify whether patient's SLC46A3 expression levels or single-nucleotide polymorphisms could impact the potency of ado-trastuzumab emtansine or other maytansine-based ADCs that are currently in clinical development. Additional studies interrogating clinical samples will be required to determine whether SLC46A3 expression can be used as a predictive biomarker of ado-trastuzumab emtansine or other ADCs containing noncleavable linker maytansines. Identification of SLC46A3, a lysosomal protein required for transport of lysine-MCC-DM1 from the lysosome to the cytoplasm could lead to the discovery of additional noncleavable linker warheads that can exit the lysosome through SLC46A3 or with other lysosomal transporters.

Disclosure of Potential Conflicts of Interest

K.J. Hamblett is a principal scientist at Amgen and has ownership interest (including patents) in Amgen stock. J.L. Gurgel has ownership interest (including patents) in Amgen. S. Siu is a senior associate scientist at Amgen and has ownership interest (including patents) in Amgen. S.P. Ragan is a senior scientist at Amgen Inc. W.S. Chang has ownership interest (including patents) in Amgen, Inc. K.C. Quon is a scientific director at Amgen. W.C. Fanslow has ownership interest (including patents) in Amgen. No potential conflicts of interest were disclosed by the other authors.

Authors' Contributions

Conception and design: K.J. Hamblett, A.P. Jacob, R.R. Milburn, D.A. Rock, M.M. Bio, K.C. Quon, W.C. Fanslow

Development of methodology: K.J. Hamblett, A.P. Jacob, J.L. Gurgel, M.E. Tometsko, B.M. Rock, S.K. Patel, S. Siu, S.P. Ragan, C.J. Borths, J.W. O'Neill, W.S. Chang, M.M. Bio, K.C. Quon, W.C. Fanslow

Acquisition of data (provided animals, acquired and managed patients, provided facilities, etc.): K.J. Hamblett, J.L. Gurgel, M.E. Tometsko, B.M. Rock, S.K. Patel, S. Siu, C.J. Borths, J.W. O'Neill, W.S. Chang, M.F. Weidner, W.C. Fanslow
Analysis and interpretation of data (e.g., statistical analysis, biostatistics, computational analysis): K.J. Hamblett, J.L. Gurgel, M.E. Tometsko, B.M. Rock, S.K. Patel, S.P. Ragan, D.A. Rock, W.S. Chang, K.C. Quon, W.C. Fanslow
Writing, review, and/or revision of the manuscript: K.J. Hamblett, A.P. Jacob, M.M. Bio, K.C. Quon, W.C. Fanslow
Administrative, technical, or material support (i.e., reporting or organizing data, constructing databases): K.J. Hamblett, S.P. Ragan
Study supervision: K.J. Hamblett, K.C. Quon, W.C. Fanslow
Other (oversight of overall research plan and execution): W.C. Fanslow

Acknowledgments

The authors thank Dr. Darrell Bigner for proving the U251vIII cells and ImmunoGen Inc. for supplying the DM1 for the anti-CD70 antibody and anti-EGFRvIII antibody conjugates. All work was performed at Amgen.

The costs of publication of this article were defrayed in part by the payment of page charges. This article must therefore be hereby marked *advertisement* in accordance with 18 U.S.C. Section 1734 solely to indicate this fact.

Received June 12, 2015; revised August 5, 2015; accepted September 17, 2015; published OnlineFirst December 2, 2015.

References

1. Senter PD, Sievers EL. The discovery and development of brentuximab vedotin for use in relapsed Hodgkin lymphoma and systemic anaplastic large cell lymphoma. Nat Biotechnol 2012;30:631–7.
2. Verma S, Miles D, Gianni L, Krop IE, Welslau M, Baselga J, et al. Trastuzumab emtansine for HER2-positive advanced breast cancer. N Engl J Med 2012;367:1783–91.
3. Mullard A. Maturing antibody-drug conjugate pipeline hits 30. Nat Rev Drug Discov 2013;12:329–32.
4. Kovtun YV, Audette CA, Ye Y, Xie H, Ruberti MF, Phinney SJ, et al. Antibody-drug conjugates designed to eradicate tumors with homogeneous and heterogeneous expression of the target antigen. Cancer Res 2006;66:3214–21.
5. Okeley NM, Miyamoto JB, Zhang X, Sanderson RJ, Benjamin DR, Sievers EL, et al. Intracellular activation of SGN-35, a potent anti-CD30 antibody-drug conjugate. Clin Cancer Res 2010;16:888–97.
6. Erickson HK, Park PU, Widdison WC, Kovtun YV, Garrett LM, Hoffman K, et al. Antibody-maytansinoid conjugates are activated in targeted cancer cells by lysosomal degradation and linker-dependent intracellular processing. Cancer Res 2006;66:4426–33.
7. Zhao RY, Wilhelm SD, Audette C, Jones G, Leece BA, Lazar AC, et al. Synthesis and evaluation of hydrophilic linkers for antibody-maytansinoid conjugates. J Med Chem 2011;54:3606–23.
8. Doronina SO, Mendelsohn BA, Bovee TD, Cerveny CG, Alley SC, Meyer DL, et al. Enhanced activity of monomethylauristatin F through monoclonal antibody delivery: effects of linker technology on efficacy and toxicity. Bioconjug Chem 2006;17:114–24.
9. Rock BM, Tometsko ME, Patel SK, Hamblett KJ, Fanslow WC, Rock DA. Intracellular catabolism of an antibody drug conjugate with a noncleavable linker. Drug Metab Dispos 2015;43:1341–4.
10. Mohr SE, Smith JA, Shamu CE, Neumuller RA, Perrimon N. RNAi screening comes of age: improved techniques and complementary approaches. Nat Rev Mol Cell Biol 2014;15:591–600.
11. Kittler R, Putz G, Pelletier L, Poser I, Heninger AK, Drechsel D, et al. An endoribonuclease-prepared siRNA screen in human cells identifies genes essential for cell division. Nature 2004;432:1036–40.
12. Yang L, Perez AA, Fujie S, Warden C, Li J, Wang Y, et al. Wnt modulates MCL1 to control cell survival in triple negative breast cancer. BMC Cancer 2014;14:124.
13. Whitehurst AW, Bodemann BO, Cardenas J, Ferguson D, Girard L, Peyton M, et al. Synthetic lethal screen identification of chemosensitizer loci in cancer cells. Nature 2007;446:815–9.
14. Xu M, Takanashi M, Oikawa K, Tanaka M, Nishi H, Isaka K, et al. USP15 plays an essential role for caspase-3 activation during Paclitaxel-induced apoptosis. Biochem Biophys Res Commun 2009;388:366–71.
15. Julien O, Kampmann M, Bassik MC, Zorn JA, Venditto VJ, Shimbo K, et al. Unraveling the mechanism of cell death induced by chemical fibrils. Nat Chem Biol 2014;10:969–76.
16. Hamblett KJ, Kozlosky CJ, Siu S, Chang WS, Liu H, Foltz IN, et al. AMG 595, an anti-EGFRvIII antibody-drug conjugate, induces potent antitumor activity against EGFRvIII-expressing glioblastoma. Mol Cancer Ther 2015;14:1614–24.
17. Nolan-Stevaux O, Tedesco D, Ragan S, Makhanov M, Chenchik A, Ruefli-Brasse A, et al. Measurement of cancer cell growth heterogeneity through lentiviral barcoding identifies clonal dominance as a characteristic of tumor engraftment. PLoS ONE 2013;8:e67316.
18. Babij C, Zhang Y, Kurzeja RJ, Munzli A, Shehabeldin A, Fernando M, et al. STK33 kinase activity is nonessential in KRAS-dependent cancer cells. Cancer Res 2011;71:5818–26.
19. Hochberg Y, Benjamini Y. More powerful procedures for multiple significance testing. Stat Med 1990;9:811–8.
20. Bagshaw RD, Mahuran DJ, Callahan JW. A proteomic analysis of lysosomal integral membrane proteins reveals the diverse composition of the organelle. Mol Cell Proteomics 2005;4:133–43.
21. Chapel A, Kieffer-Jaquinod S, Sagne C, Verdon Q, Ivaldi C, Mellal M, et al. An extended proteome map of the lysosomal membrane reveals novel potential transporters. Mol Cell Proteomics 2013;12:1572–88.
22. Schroder B, Wrocklage C, Pan C, Jager R, Kosters B, Schafer H, et al. Integral and associated lysosomal membrane proteins. Traffic 2007;8:1676–86.
23. Qiu A, Jansen M, Sakaris A, Min SH, Chattopadhyay S, Tsai E, et al. Identification of an intestinal folate transporter and the molecular basis for hereditary folate malabsorption. Cell 2006;127:917–28.
24. Kim MG, Flomerfelt FA, Lee KN, Chen C, Schwartz RH. A putative 12 transmembrane domain cotransporter expressed in thymic cortical epithelial cells. J Immunol 2000;164:3185–92.
25. Obermann H, Wingbermuhle A, Munz S, Kirchhoff C. A putative 12-transmembrane domain cotransporter associated with apical membranes of the epididymal duct. J Androl 2003;24:542–56.
26. Su AI, Wiltshire T, Batalov S, Lapp H, Ching KA, Block D, et al. A gene atlas of the mouse and human protein-encoding transcriptomes. Proc Natl Acad Sci U S A 2004;101:6062–7.
27. Wu C, Orozco C, Boyer J, Leglise M, Goodale J, Batalov S, et al. BioGPS: an extensible and customizable portal for querying and organizing gene annotation resources. Genome Biol 2009;10:R130.
28. Zhao R, Unal ES, Shin DS, Goldman ID. Membrane topological analysis of the proton-coupled folate transporter (PCFT-SLC46A1) by the substituted cysteine accessibility method. Biochemistry 2010;49:2925–31.
29. Nicholas MK, Lukas RV, Jafri NF, Faoro L, Salgia R. Epidermal growth factor receptor - mediated signal transduction in the development and therapy of gliomas. Clin Cancer Res 2006;12:7261–70.
30. Lewis Phillips GD, Li G, Dugger DL, Crocker LM, Parsons KL, Mai E, et al. Targeting HER2-positive breast cancer with trastuzumab-DM1, an antibody-cytotoxic drug conjugate. Cancer Res 2008;68:9280–90.
31. Sanderson RJ, Hering MA, James SF, Sun MM, Doronina SO, Siadak AW, et al. In vivo drug-linker stability of an anti-CD30 dipeptide-linked auristatin immunoconjugate. Clin Cancer Res 2005;11:843–52.
32. Hamblett KJ, Senter PD, Chace DF, Sun MM, Lenox J, Cerveny CG, et al. Effects of drug loading on the antitumor activity of a monoclonal antibody drug conjugate. Clin Cancer Res 2004;10:7063–70.
33. Dubowchik GM, Firestone RA, Padilla L, Willner D, Hofstead SJ, Mosure K, et al. Cathepsin B-labile dipeptide linkers for lysosomal release of doxorubicin from internalizing immunoconjugates: model studies of enzymatic drug release and antigen-specific in vitro anticancer activity. Bioconjug Chem 2002;13:855–69.
34. Sun X, Widdison W, Mayo M, Wilhelm S, Leece B, Chari R, et al. Design of antibody-maytansinoid conjugates allows for efficient detoxification via liver metabolism. Bioconjug Chem 2011;22:728–35.
35. Chari RV, Miller ML, Widdison WC. Antibody-drug conjugates: an emerging concept in cancer therapy. Angew Chem 2014;53:3796–827.

Published OnlineFirst December 2, 2015; DOI: 10.1158/0008-5472.CAN-15-1610

36. Erickson HK, Widdison WC, Mayo MF, Whiteman K, Audette C, Wilhelm SD, et al. Tumor delivery and in vivo processing of disulfide-linked and thioether-linked antibody-maytansinoid conjugates. Bioconjug Chem 2010;21:84–92.
37. Bhinder B, Djaballah H. A decade of RNAi screening: too much hay and very few needles. Drug Discov World 2013:31–41.
38. Bassik MC, Kampmann M, Lebbink RJ, Wang S, Hein MY, Poser I, et al. A systematic mammalian genetic interaction map reveals pathways underlying ricin susceptibility. Cell 2013;152:909–22.
39. Kell DB, Dobson PD, Bilsland E, Oliver SG. The promiscuous binding of pharmaceutical drugs and their transporter-mediated uptake into cells: what we (need to) know and how we can do so. Drug Discov Today 2013;18:218–39.
40. Lanthaler K, Bilsland E, Dobson PD, Moss HJ, Pir P, Kell DB, et al. Genome-wide assessment of the carriers involved in the cellular uptake of drugs: a model system in yeast. BMC Biol 2011;9:70.
41. Reiling JH, Clish CB, Carette JE, Varadarajan M, Brummelkamp TR, Sabatini DM. A haploid genetic screen identifies the major facilitator domain containing 2A (MFSD2A) transporter as a key mediator in the response to tunicamycin. Proc Natl Acad Sci U S A 2011;108:11756–65.
42. Winter GE, Radic B, Mayor-Ruiz C, Blomen VA, Trefzer C, Kandasamy RK, et al. The solute carrier SLC35F2 enables YM155-mediated DNA damage toxicity. Nat Chem Biol 2014;10:768–73.
43. Shayeghi M, Latunde-Dada GO, Oakhill JS, Laftah AH, Takeuchi K, Halliday N, et al. Identification of an intestinal heme transporter. Cell 2005;122:789–801.
44. Desmoulin SK, Hou Z, Gangjee A, Matherly LH. The human proton-coupled folate transporter: Biology and therapeutic applications to cancer. Cancer Biol Ther 2012;13:1355–73.
45. Nevo Y, Nelson N. The NRAMP family of metal-ion transporters. Biochim Biophys Acta 2006;1763:609–20.
46. Nakamura N, Lill JR, Phung Q, Jiang Z, Bakalarski C, de Maziere A, et al. Endosomes are specialized platforms for bacterial sensing and NOD2 signalling. Nature 2014;509:240–4.
47. Lam-Yuk-Tseung S, Picard V, Gros P. Identification of a tyrosine-based motif (YGSI) in the amino terminus of Nramp1 (Slc11a1) that is important for lysosomal targeting. J Biol Chem 2006;281:31677–88.
48. Bonifacino JS, Traub LM. Signals for sorting of transmembrane proteins to endosomes and lysosomes. Annu Rev Biochem 2003;72:395–447.
49. Hamann PR, Hinman LM, Hollander I, Beyer CF, Lindh D, Holcomb R, et al. Gemtuzumab ozogamicin, a potent and selective anti-CD33 antibody-calicheamicin conjugate for treatment of acute myeloid leukemia. Bioconjug Chem 2002;13:47–58.
50. Kung Sutherland MS, Walter RB, Jeffrey SC, Burke PJ, Yu C, Kostner H, et al. SGN-CD33A: a novel CD33-targeting antibody-drug conjugate using a pyrrolobenzodiazepine dimer is active in models of drug-resistant AML. Blood 2013;122:1455–63.

Cancer Research
The Journal of Cancer Research (1916–1930) | The American Journal of Cancer (1931–1940)

AACR American Association for Cancer Research

SLC46A3 Is Required to Transport Catabolites of Noncleavable Antibody Maytansine Conjugates from the Lysosome to the Cytoplasm

Kevin J. Hamblett, Allison P. Jacob, Jesse L. Gurgel, et al.

Cancer Res 2015;75:5329-5340. Published OnlineFirst December 2, 2015.